Integrated noncollinear red–green–blue laser light source using a two-dimensional nonlinear photonic quasicrystal

Lina Zhao, Zhen Qi, Ye Yuan, Jun Lu, Yanhua Liu, Changdong Chen, Xinjie Lv, Zhenda Xie, Xiaopeng Hu,* Gang Zhao, Ping Xu, and Shining Zhu

National Laboratory of Solid State Microstructures and Department of Physics, Nanjing University, Nanjing, 210093 China
**Corresponding author: xphu@nju.edu.cn*

Received November 19, 2010; revised January 17, 2011; accepted January 18, 2011; posted January 21, 2011 (Doc. ID 138477); published March 2, 2011

We report on a noncollinear red–green–blue (RGB) laser light source using a two-dimensional nonlinear photonic quasicrystal. The red and blue lights result from a green light pumped optical parametric generation process cascading two frequency doubling processes in a single-pass setup. Together with the residual green light, two sets of RGB lights were observed in a wide temperature range, which indicates a practical method for constructing a compact multiwavelength laser light source.

OCIS codes: 190.4410, 140.7300, 190.4400.

1. INTRODUCTION

In nonlinear optics, due to material dispersion, efficient nonlinear interactions require compensation for phase mismatches between the interacting waves. The dielectric superlattice has been proved as a promising material for frequency conversion in terms of quasi-phase-matching (QPM) [1–3]. The so-called $\chi^{(2)}$ modulated crystal is QPM material that uses spatial modulation of the relevant component of a nonlinear susceptibility tensor to compensate the phase mismatch for efficient frequency conversion. Usually, a one-dimensional (1D) periodic structure can provide a basic reciprocal vector and typically phase match only one collinear process [4,5]. In recent years, the method of simultaneously phase matching several nonlinear processes has been applied in fields such as the creation of multiple radiation sources [6], multicolored solitons [7], and multiple entanglement sources [8,9]. Two or more nonlinear optical processes and noncollinear interactions typically require more complex QPM structures. Two-dimensional (2D) periodic crystals [10–16] and 2D nonlinear photonic quasicrystals (2DNPQCs) are available. The reason is that they can provide a wealth of reciprocal lattice vectors that are able to compensate for phase mismatches in multiple nonlinear processes. One method of constructing a 2DNPQC is based on Penrose tiling, proposed in quasicrystal by Penrose [17]. Several works have been made, such as noncollinear second harmonic generations (SHGs) [18,19]. This method has limited flexibility, and it could not arbitrarily phase match multiple frequency conversion processes. Another method is based on the generalized dual-grid method (GDGM) [20–24], which allows the structure to simultaneously phase match any arbitrary set of frequency conversion processes in any special direction [20]. It is flexible and realizes multiple nonlinear interactions in a single crystal. The GDGM can be used to generate any of the structures and has the advantage of generating a much wider class of patterns than the other methods [25].

In this work, we demonstrate a 2DNPQC to phase match three frequency conversion processes based on the GDGM. One collinear optical parametric generation (OPG) process cascading two noncollinear frequency doubling processes of the signal and idler are realized, generating two sets of red and blue light in a single-pass setup. Experimental results, including temperature and spectral detuning characteristics of the 2DNPQC, are also studied.

2. STRUCTURE DESIGN

The OPG process was frequency downconverted from 532 to 918 and 1266 nm, and frequency doubling of the signal and idler was 459 for the blue and 633 nm for red lights. We chose $LiTaO_3$ as the nonlinear crystal, and the phase-matching temperature was set to be 180 °C. The corresponding wave vector mismatches for the three processes can be described as $\Delta\mathbf{k}_1$, $\Delta\mathbf{k}_2$, and $\Delta\mathbf{k}_3$, which are 2D vectors in reciprocal space. The components of $\Delta\mathbf{k}_1$, $\Delta\mathbf{k}_2$, and $\Delta\mathbf{k}_3$ can be described as $(\Delta k_{11}, \Delta k_{12})$, $(\Delta k_{21}, \Delta k_{22})$, and $(\Delta k_{31}, \Delta k_{32})$ respectively. According to the GDGM [20], they can be viewed as two three-dimensional (3D) vectors $(\Delta k_{11}, \Delta k_{21}, \Delta k_{31})$ and $(\Delta k_{12}, \Delta k_{22}, \Delta k_{32})$. By adding the third 3D vector $\mathbf{q}_j = (q_1, q_2, q_3)$, orthogonal to $(\Delta k_{11}, \Delta k_{21}, \Delta k_{31})$ and $(\Delta k_{12}, \Delta k_{22}, \Delta k_{32})$, we complete it so it becomes a basis of the 3D space $\mathbf{K}_j = (\Delta\mathbf{k}_j, \mathbf{q}_j)$ $(j = 1, 2, 3)$. $\mathbf{K}_j$ is a 3×3 matrix, written as

$$\mathbf{K}_j = \begin{bmatrix} \Delta k_{11} & \Delta k_{12} & q_1 \\ \Delta k_{21} & \Delta k_{22} & q_2 \\ \Delta k_{31} & \Delta k_{32} & q_3 \end{bmatrix}. \quad (1)$$

Then we can find three basis vectors in real space, denoted

$$\mathbf{A}_j = \begin{bmatrix} a_{11} & a_{12} & b_1 \\ a_{21} & a_{22} & b_2 \\ a_{31} & a_{32} & b_3 \end{bmatrix}. \quad (2)$$

The orthogonality condition is satisfied by $\mathbf{A}_i \cdot \mathbf{K}_j = 2\pi\delta_{ij}$. In Eq. (2) $\mathbf{A}_j = (\mathbf{a}_j, \mathbf{b}_j)$. $\mathbf{a}_j$ are called 2D tiling vectors, and they can be written as

$$\mathbf{a}_j = \begin{bmatrix} a_{11} & a_{12} \\ a_{21} & a_{22} \\ a_{31} & a_{32} \end{bmatrix}, \quad (3)$$

while $\mathbf{b}_j$ are the 3D vectors in real space. The reciprocal vectors $\mathbf{q}_j$ are not unique, but once chosen, the tiling vectors $\mathbf{a}_j$ and the extension $\mathbf{b}_j$ are uniquely determined by the orthogonality condition. The three basic vectors $\mathbf{a}_1$, $\mathbf{a}_2$, and $\mathbf{a}_3$ in 2D real space are called tiling vectors, which construct three types of parallelograms (tiling) that can overspread the whole quasiperiod lattice, as shown in Fig. 1. The circular motifs in Fig. 1(a) represent the nonlinear tensor component of the polarization with a negative value: $-\chi^{(2)}$. The background is made with positive polarization $+\chi^{(2)}$. The centers between the two nearby circles constitute a tiling vector. The radius is optimized by a numerical procedure to be 2.3 μm for the best Fourier coefficients for the three desired processes. The magnitudes of $\mathbf{a}_1$, $\mathbf{a}_2$, and $\mathbf{a}_3$ are 16.4, 11.3, and 6 μm, respectively.

Figure 2(a) is the Fourier transformation of the structure with the size of the dots representing the size of the Fourier coefficients. Figure 2(b) shows the phase-matching geometry for multiple frequency conversions. The reciprocal vector $\mathbf{G}_1 = \Delta\mathbf{k}_1 = \mathbf{k}_p - \mathbf{k}_s - \mathbf{k}_i$ is parallel to x axis and compensates for the phase mismatch $\Delta\mathbf{k}_1$ in OPG. The QPM conditions for the two SHG processes can be written as $\mathbf{k}_{2\omega} - \mathbf{k}_\omega - \mathbf{G}_i = 0$ for $i = 2, 3$, where $\mathbf{G}_2$ and $\mathbf{G}_3$ are the reciprocal vectors that compensate for phase mismatches $\Delta\mathbf{k}_2$ and $\Delta\mathbf{k}_3$ for each SHG process and $\mathbf{k}_\omega$ and $\mathbf{k}_{2\omega}$ are the wave vectors of the parametric and second-harmonic (SH) waves, respectively. The two SHG processes generate noncollinear blue and red beams, which means that there is an angle between the fundamental and harmonic beams. The magnitudes and angles are 0.84 μm^{-1}, $\angle$0 rad for $\mathbf{G}_1$; 1.45 μm^{-1}, $\angle$0.42 rad for $\mathbf{G}_2$; and 0.51 μm^{-1}, $\angle$0.13 rad for $\mathbf{G}_3$, respectively. The detailed

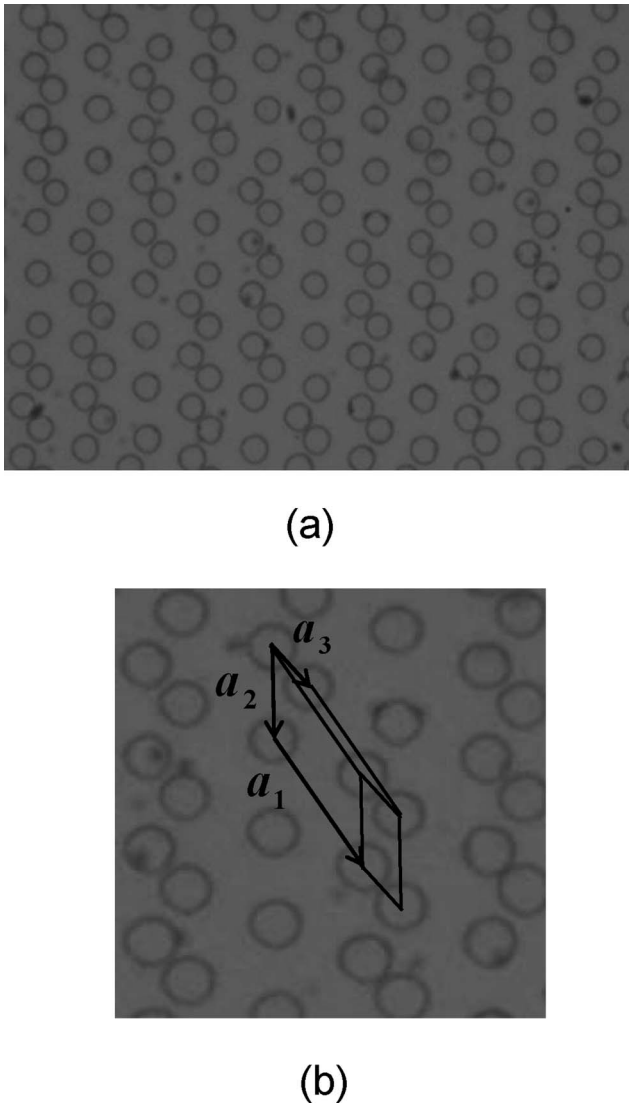

Fig. 1. (Color online) (a) $+z$ face micrograph of the quasiperiodically poled LT after being slightly etched in HF acid. (b) Detailed view of the domain pattern, which gives three types of parallelograms.

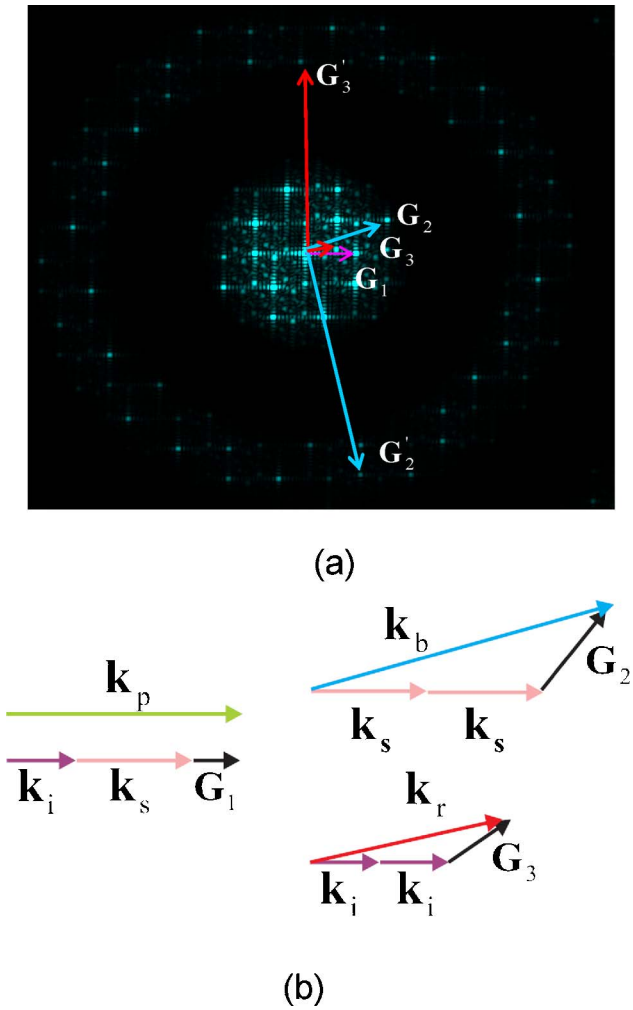

Fig. 2. (Color online) (a) Reciprocal space of the quasiperiodically poled LT. (b) The phase-matching geometry for multiple frequency conversions.

Table 1. Calculated Mismatch Vectors for Optical Parametric Generation and Frequency Doubling Processes

Mismatch Vector	Magnitude in $(\mu m)^{-1}$	Direction in Radians	$g(\Delta \mathbf{k}_i)^a$
$\Delta \mathbf{k}_1 = \mathbf{G}_1$	0.81568	0	0.2117
$\Delta \mathbf{k}_2 = \mathbf{G}_2$	1.45164	0.42	0.0989
$\Delta \mathbf{k}_3 = \mathbf{G}_3$	0.51020	0.13	0.0811

[a]Fourier coefficients for the three processes.

characteristics of the reciprocal vectors and tiling vectors are given in Tables 1 and 2.

3. RESULTS AND DISCUSSIONS

The 2DNPQC was fabricated by electric-field poling a z-cut $LiTaO_3$ (LT) wafer at room temperature. The poled LT sample was 0.5 mm in thickness, 3 mm in width, and 35 mm in length. The optimized poled ratio was 0.32 in calculation; thus, during poling, the poled ratio was controlled to be 0.32. The sample was slightly etched in hydrofluoric (HF) acid to reveal the domain pattern, and the $+z$ surface micrograph of the sample is shown in Fig. 1(a). The near circularly inverted domains with a radius of 2.9 μm distribute in the $+\chi^{(2)}$ background, which indicates it is a little overpoled compared with the theoretical calculation radius of 2.3 μm. Figure 1(b) is the detailed view of the pattern, which clearly gives three types of parallelograms constructed by the three basic vectors $\mathbf{a}_1$, $\mathbf{a}_2$, and $\mathbf{a}_3$.

The pump source was a 10 Hz, 532 nm green laser with a pulse duration of 3.5 ns and a linewidth of 0.1 nm. A lens with a focal length of $f = 150$ mm was used to focus the z-polarized pump light into the crystal, and the beam waist inside the crystal was estimated to be about 120 μm. The crystal was embedded in an oven with an accuracy of 0.1 °C. The oven was used in a single-pass setup.

The pump beam was incident on the crystal along the direction of $\mathbf{G}_1$, and a parametric downconversion process happened when the momentum conservation was ensured by $\mathbf{G}_1 = \mathbf{k}_p - \mathbf{k}_s - \mathbf{k}_i$. By carefully aligning the setup, we could get a maximum output energy of the signal and idler to make sure the pump beam was incident along $\mathbf{G}_1$ and the generated signal and idle light were both collinear with the pump light. When the crystal temperature was tuned from 110 °C to 200 °C, the wavelength of the signal light varied from 986.9 to 890.6 nm, which covered about 96 nm, while the idle light covered a wide spectrum of 167 nm from 1154.2 to 1321.3 nm. The measured temperature tuning curves for both the signal and idler are shown in Fig. 3, which is well accordant with the theoretical calculation.

Second harmonic generations of the signal and idler happened when momentum conservations satisfied the conditions $\mathbf{k}_b - \mathbf{k}_s - \mathbf{k}_s - \mathbf{G}_2 = 0$ and $\mathbf{k}_r - \mathbf{k}_i - \mathbf{k}_i - \mathbf{G}_3 = 0$, respectively. The energy of the blue light reached its maximum at

Table 2. Detailed characteristics of the Tiling Vectors

Tiling Vector	Magnitude in μm	Direction in Radians
$\mathbf{a}_1$	16.4	−1.16
$\mathbf{a}_2$	11.3	−1.54
$\mathbf{a}_3$	6.0	−1.09

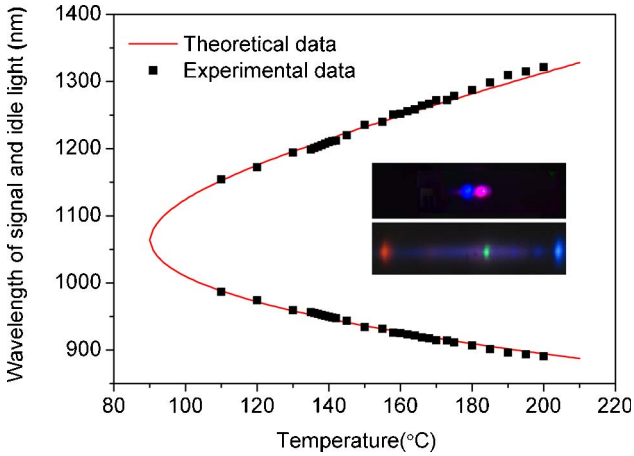

Fig. 3. (Color online) Temperature-dependent curve for the OPG process. Insets, photographs of the signal harmonics participant by $\mathbf{G}_2$ or $\mathbf{G}_2'$ and the idle harmonics participant by $\mathbf{G}_3$ or $\mathbf{G}_3'$ when filtering out most of the pump beam.

167 °C, as shown in Fig. 4, and the fitted temperature full-width at half-maximum (FWHM) was about 13.0 °C. When lowering the temperature to 165 °C, the red energy reached

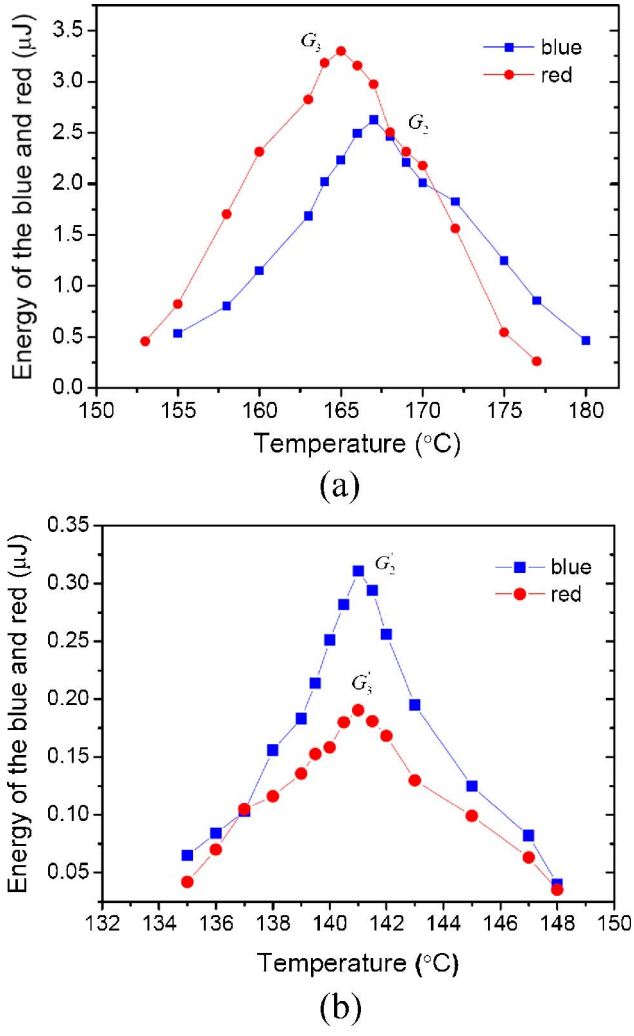

Fig. 4. (Color online) Measured temperature tuning curves for each set of the frequency self-doubling process (a) using $\mathbf{G}_2$ and $\mathbf{G}_3$ and (b) using $\mathbf{G}_2'$ and $\mathbf{G}_3'$.

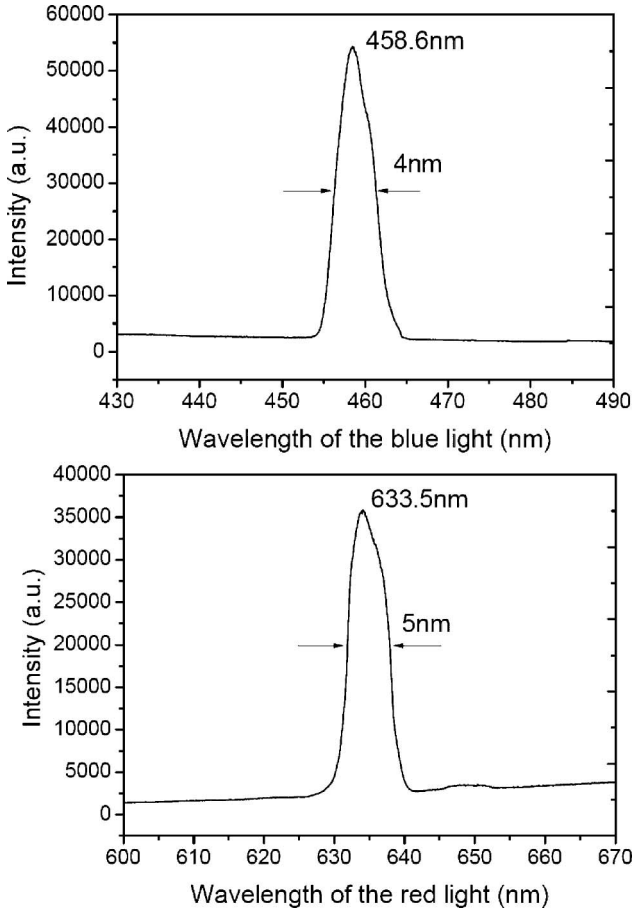

Fig. 5. Measured spectra of the blue and red lights at 166 °C, respectively.

its peak and the fitted temperature FWHM was 13.7 °C. Both of the SHG temperature bandwidths were rather bigger than that in a 1D periodic structure, which mainly resulted from the noncollinear phase-matching characteristics in the 2D quasi-periodically poled structure [17].

The temperature tuning curves of the two SHG processes crossed at 166 °C. At this temperature point, the signal and idler wavelengths were 917 and 1267 nm, and the corresponding linewidth were 6.3 and 12 nm, respectively. The harmonic of the signal produced a blue spot with an external angle of 0.0280 rad (theoretical, 0.0192 rad). The corresponding central wavelength was 458.6 nm, and the linewidth was 4 nm. Red light generated from frequency doubling of the idle light had an output angle of 0.0035 rad (theoretical, 0.0052 rad), the central wavelength was 633.5 nm and the linewidth was 5 nm. Figure 5 gives the measured spectra of the blue and red lights, respectively. The energy of the signal and idle lights and their corresponding SH waves increased with the increasing pump energy. When the pump energy reached 0.8 mJ, a total energy of 157 μJ of both signal and idle lights was obtained. The conversion efficiency of the total output energy of the signal and idle over pump energy was 19.6%. The energies of the blue and red lights were 2.63 and 3.3 μJ, respectively. The generated red and blue light together with the residual green beam composed the red–green–blue (RGB) laser source.

When the temperature was lowered to 144 °C, another set of frequency doublings of the signal and idler occurred. The reciprocal lattice vectors $\mathbf{G}_2'$ and $\mathbf{G}_3'$ were used to satisfy the momentum conservations in the two SHG processes. From the theoretical calculation, $|\mathbf{G}_2'| = 4.38\,\mu\text{m}^{-1}$ and the angle between vector $\mathbf{G}_1$ and $\mathbf{G}_2'$ was 1.34 rad. $|\mathbf{G}_3'| = 3.4\,\mu\text{m}^{-1}$, and the angle between $\mathbf{G}_1$ and $\mathbf{G}_3'$ was 1.5 rad. The energy of the blue and red both reached the maximum at 141 °C, and the measured wavelength of the signal and idler were 948.5 and 1211.5 nm, respectively. The corresponding wavelengths of blue and red were 474.2 and 605.8 nm, respectively, and the output angles for blue and red beams become larger toward 0.145 and 0.166 rad, respectively, due to the larger reciprocal vectors got involved. The energy of blue and red were 0.3 and 0.19 μJ, respectively, which showed a lower efficiency than frequency doubling using $\mathbf{G}_2$ and $\mathbf{G}_3$. This is mainly due to the much lower Fourier coefficients of $\mathbf{G}_2'$ and $\mathbf{G}_3'$ compared with that of $\mathbf{G}_2$ and $\mathbf{G}_3$.

Figure 4 shows the temperature tuning curves for each set of frequency doubling processes. From Fig. 4(a), we can see the temperature for maximum output of red and blue deviates a little from each other, and the temperature bandwidths are both around 10 °C. Figure 4(b) shows the tuning curves of another set of blue and red, and the temperature bandwidths are 5.5 °C and 7.0 °C. Thus, the two sets of blue and red beams can both occur within a wide temperature range. In 2D periodically poled structures, it could hardly be realized because only one freedom, i.e., the lattice parameter, can be chosen to meet multiple phase-matching conditions [16].

It is worth noting that we observed two sets of noncollinear RGB beams in the experiment, and these two sets of RGB laser light can cover most of the area in the Commission International de l'Eclairage (CIE) chromaticity diagram. Because the signal and idler beams are both collinear with the pump beam, it is easy to realize singly or doubly resonant optical parametric oscillation, thus providing the signal or idler higher feedback for more efficient red–blue output from the 2DNPQC.

4. SUMMARY

In conclusion, we have designed and fabricated a 2DNPQC based on the GDGM. A collinear OPG process cascading two noncollinear SHGs of the pregenerated signal and idler wavelengths are realized in a single crystal. Two sets of red–blue light are obtained when tuning the temperature. The generated red–blue lights, together with the residual green pump light, compose a noncollinear three elemental colors in vision. This scheme has potential applications in laser displays and quantum optics [9].

ACKNOWLEDGMENTS

This work was supported by the National Natural Science Foundation of China (NSFC) (under grants 11021403, 10904066, and NSAF10776011) and the State Key Program for Basic Research of China (under grants 2011CBA00205 and 2010CB630703).

REFERENCES

1. J. A. Armstrong, N. Bloembergen, J. Ducuing, and P. S. Pershan, "Interactions between light waves in a nonlinear dielectric," Phys. Rev. **127**, 1918–1939 (1962).

2. M. M. Fejer, G. A. Magel, D. H. Hundt, and R. L. Byer, "Quasi-phase-matched second harmonic generation: tuning and tolerances," IEEE J. Quantum Electron. **28**, 2631–2654 (1992).
3. S. N. Zhu, Y. Y. Zhu, and N. B. Ming, "Quasi-phase-matched third-harmonic generation in a quasi-periodic optical superlattice," Science **278**, 843–846 (1997).
4. M. Yamada, N. Nada, M. Saitoh, and K. Watanabe, "First-order quasi-phase matched $LiNbO_3$ waveguide periodically poled by applying an external field for efficient blue second-harmonic generation," Appl. Phys. Lett. **62**, 435–436 (1993).
5. G. D. Miller, R. G. Batchko, W. M. Tulloch, D. R. Weise, M. M. Fejer, and R. L. Byer, "42%-efficient single-pass cw second-harmonic generation in periodically poled lithium niobate," Opt. Lett. **22**, 1834–1836 (1997).
6. S. N. Zhu, Y. Y. Zhu, Y. Q. Qin, H. F. Wang, C. Z. Ge, and N. B. Ming, "Experimental realization of second harmonic generation in a Fibonacci optical superlattice of $LiTaO_3$," Phys. Rev. Lett. **78**, 2752–2755 (1997).
7. Y. S. Kivshar, A. A. Sukhorukov, and S. M. Saltiel, "Two-color multistep cascading and parametric soliton-induced waveguides," Phys. Rev. E **60**, R5056–R5059 (1999).
8. P. C. Pooser and O. Pfister, "Observation of triply coincident nonlinearities in periodically poled $KTiOPO_4$," Opt. Lett. **30**, 2635–2637 (2005).
9. O. Pfister, S. Feng, G. Jennings, R. Pooser, and D. Xie, "Multipartite continuous-variable entanglement from concurrent nonlinearities," Phys. Rev. A **70**, 020302 (2004).
10. V. Berger, ""Nonlinear photonic crystals," Phys. Rev. Lett. **81**, 4136–4139 (1998).
11. N. G. R. Broderick, G. W. Ross, H. L. Offerhaus, D. J. Richardson, and D. C. Hanna, "Hexagonally poled lithium niobate: a two-dimensional nonlinear photonic crystal," Phys. Rev. Lett. **84**, 4345–4348 (2000).
12. P. G. Ni, B. Q. Ma, X. H. Wang, B. Y. Cheng, and D. Z. Zhang, "Second-harmonic generation in two-dimensional periodically poled lithium niobate using second-order quasiphase matching," Appl. Phys. Lett. **82**, 4230–4232 (2003).
13. L.-H. Peng, C.-C. Hsu, and Y.-C. Shih, "Second-harmonic green generation from two-dimensional $\chi^{(2)}$ nonlinear photonic crystal with orthorhombic lattice structure," Appl. Phys. Lett. **83**, 3447–3449 (2003).
14. N. Fujioka, S. Ashihara, H. Ono, T. Shimura, and K. Kuroda, "Cascaded third-harmonic generation of ultrashort optical pulses in two-dimensional quasi-phase-matching gratings," J. Opt. Soc. Am. B **24**, 2394–2405 (2007).
15. P. Xu, S. H. Ji, S. N. Zhu, X. Q. Yu, J. Sun, H. T. Wang, J. L. He, Y. Y. Zhu, and N. B. Ming, "Conical second harmonic generation in a two-dimensional $\chi^{(2)}$ photonic crystal: a hexagonally poled $LiTaO_3$ crystal," Phys. Rev. Lett. **93**, 133904 (2004).
16. P. Xu, Z. D. Xie, H. Y. Leng, J. S. Zhao, J. F. Wang, X. Q. Yu, Y. Q. Qin, and S. N. Zhu, "Frequency self-doubling optical parametric amplification: noncollinear red-green-blue light-source generation based on a hexagonally poled lithium tantalate," Opt. Lett. **33**, 2791–2793 (2008).
17. R. Penrose, in *The Physics of Quasicrystals*, P. J. Steinhardt and S. Ostund, eds. (World Scientific, 1987), App. I.
18. B. Q. Ma, T. Wang, Y. Sheng, P. G. Ni, Y. Q. Wang, B. Y. Cheng, and D. Z. Zhang, "Quasiphase matched harmonic generation in a two-dimensional octagonal photonic superlattice," Appl. Phys. Lett. **87**, 251103 (2005).
19. R. T. Bratfalean, A. C. Peacock, N. G. R. Broderick, K. Gallo, and R. Lewen, "Harmonic generation in a two-dimensional nonlinear quasi-crystal," Opt. Lett. **30**, 424–426 (2005).
20. R. Lifshitz, A. Arie, and A. Bahabad, "Photonic quasicrystals for nonlinear optical frequency conversion," Phys. Rev. Lett. **95**, 133901 (2005).
21. D. A. Rabson, T.-L. Ho, and N. D. Mermin, "Aperiodic tilings with non-symmorphic space groups $p2_1^1gm$," Acta Crystallogr. **44**, 678–688 (1988).
22. F. Gahler and J. Rhyner, "Equivalence of the generalized grid and projection methods for the construction of quasiperiodic tilings," J. Phys. A **19**, 267–277 (1986).
23. A. Bahabad, N. Voloch, A. Arie, and R. Lifshitz, "Experimental confirmation of the general solution to the multiple-phase-matching problem," J. Opt. Soc. Am. B **24**, 1916–1921 (2007).
24. A. Bahabad, A. Ganany-Padowicz, and A. Arie, "Enginneering two-dimensional nonlinear photonic quasi-crystals," Opt. Lett. **33**, 1386–1388 (2008).
25. J. E. S. Socolar, P. J. Sternhardt, and D. Levine, "Quasicrystals with arbitrary orientational symmetry," Phys. Rev. B **32**, 5547–5550 (1985).